Heliyon 9 (2023) e13191

Contents lists available at ScienceDirect

Heliyon

journal homepage: www.cell.com/heliyon

Research article

Hsa_circ_0072309 is a prognostic biomarker and is correlated with immune infiltration in gastric cancer

Bei-Bei Xu [a,b,c], Yi Huang [d], En-Dian Zheng [b], Jing-Ya Wang [c], Chen-Jing Zhang [c], Xiao-Ge Geng [c], Ya-Nan Wang [e], Wen-Sheng Pan [a,c,f,*]

[a] Suzhou Medical College of Soochow University, Suzhou, Jiangsu, 215000, China
[b] Department of Gastroenterology, Wenzhou Third Clinical Institute Affiliated to Wenzhou Medical University, The Third Affiliated Hospital of Shanghai University, Wenzhou People's Hospital, Wenzhou, 325000, Zhejiang, China
[c] Department of Gastroenterology, Zhejiang Provincial People's Hospital, Hangzhou, 310000, Zhejiang, China
[d] Department of General Surgery, Wenzhou Third Clinical Institute Affiliated to Wenzhou Medical University, The Third Affiliated Hospital of Shanghai University, Wenzhou People's Hospital, Wenzhou, 325000, Zhejiang, China
[e] Zhejiang University of Technology, Hangzhou, 310000, Zhejiang, China
[f] People's Hospital of Hangzhou Medical College, Hangzhou, 310000, Zhejiang, China

ARTICLE INFO

Keywords:
Gastric cancer
Circular RNA
Immune infiltration
Lymph node metastasis
Complement component 7

ABSTRACT

Background: Hsa_circ_0072309 has been identified as a tumor suppressor in several carcinomas. However, its precise role in gastric cancer (GC) remains largely unknown. This study was aimed to explore the precise role of Hsa_circ_0072309 in GC.

Methods: The transcriptional and clinical data of stomach adenocarcinoma were downloaded using the University of California SantaCruz (UCSC) Xena browser. The circular RNA (circRNA) datasets were obtained from the Gene Expression Omnibus (GEO) database. The expression profile and survival analysis of differentially expressed micro RNAs (DEMIs) and differentially expressed messenger RNAs (DEMs) were performed. Correlations between the expression and immune infiltration of the DEMS were studied. Additionally, the expression of hsa_circ_0072309 in GC tissues and cell lines were validated, and the relationship between its expression and clinical features was investigated. Gain- and loss-of function experiments and molecular interaction experiments were also conducted.

Results: Overall, 7 differentially expressed circRNAs, 13 DEMIs, and 17 DEMs were screened. Two DEMIs (hsa_miR-34a-3p and hsa_miR-326) and five DEMs (C7, MARCKSL1, UBE2T, OLR1, and HOXC11) showed significant differences in the high- and low-risk groups. The most significantly enriched Gene Ontology terms were the circadian regulation of gene expression and protein binding. The most significantly enriched Kyoto Encyclopedia of Genes and Genomes pathways were the PI3K-Akt and Ras signal pathways. Additionally, six genes were significantly correlated with immune infiltration. The real-time quantitative PCR (RT-qPCR) results revealed a significant downregulation of hsa_circ_0072309 in GC tissues related to tumor size, vascular invasion, and lymph node metastasis. A hsa_circ_0072309 overexpression suppressed whereas a hsa_circ_0072309 knockdown promoted GC cells proliferation and migration in vitro; in addition, hsa_circ_0072309 could directly bind to has-miR-34a-3p and has-miR-330-5p.

* Corresponding author. Department of Gastroenterology, Zhejiang Provincial People's Hospital, Hangzhou, 310000, Zhejiang, China.
E-mail address: wspan223@163.com (W.-S. Pan).

https://doi.org/10.1016/j.heliyon.2023.e13191
Received 11 August 2022; Received in revised form 16 January 2023; Accepted 19 January 2023
Available online 4 February 2023
2405-8440/© 2023 The Authors. Published by Elsevier Ltd. This is an open access article under the CC BY-NC-ND license (http://creativecommons.org/licenses/by-nc-nd/4.0/).

Conclusions: Hsa_circ_0072309 is a potential diagnostic biomarker for GC, and complement component 7 may be a tumor suppressor. These may potentially predict the prognosis of patients with GC and may become new therapeutic targets.

1. Introduction

Globally, gastric cancer (GC) remains a significant cause of cancer-related deaths among gastrointestinal malignancies. Although its morbidity and mortality have declined in recent decades [1], GC has a high annual incidence of 1 million cases and nearly 800,000 deaths worldwide [2]. The atypical symptoms of early GC and the lack of specific diagnostic biomarkers explain why most GC patients are diagnosed at an advanced stage [3]. Advanced GC has higher metastasis rates and a worse prognosis, with a five-year survival rate lower than 20% [4]. Therefore, it is essential to study the molecular mechanisms of the occurrence and development of GC; it is also necessary to find the molecular targets that can block tumor progression.

Circular RNAs (circRNAs) have been identified as new competing endogenous RNAs (ceRNAs), which can act as microRNA (miRNA) sponges to competitively bind to miRNAs [5]. Recently, the epigenetic regulatory role of circRNAs in GC development has been increasingly recognized. The ceRNA axis is the most studied mechanism of GC genesis and progression [6]. Peng et al. [7] found that circCUL2 might inhibit cancer progression and regulate cisplatin sensitivity through autophagy activation mediated by has_miR-142-3p/rock2. Rong et al. [8] reported that circPSMC3 suppressed the proliferation and metastasis in GC via the ceRNA axis. Similarly, hsa_circ_0066444 also promoted proliferation, invasion, and migration [9] via the ceRNA axis.

Our group's previous study found that hsa_circ_0072309 was down-regulated in GC tissue by circRNA microarray analysis and that it had a high diagnostic value in GC, especially in poorly differentiated adenocarcinoma [10]. Guo et al. [11] found that hsa_circ_0072309 could inhibit the growth of the GC cell line AGS by suppressing the PI3K-AKT signaling pathway through activation of the PPARγ-PTEN signaling pathway. However, the mechanism of how hsa_circ_0072309 interacts with the ceRNA axis in GC remains unclear. Most studies on circRNAs in GC were based on bioinformatics analysis and lack in-depth experimental verification. Additionally, most studies were reported from a single center and have small sample sizes. Furthermore, few studies have focused on the integrative analysis of one single circRNA in ceRNA, including the expression or prognosis analysis of its downstream miRNAs or messenger RNAs (mRNAs) and the correlation among differentially expressed mRNAs (DEMs), clinical characteristics, and immune infiltration.

In this paper, a comprehensive analysis of the mechanism of hsa_circ_0072309 as a ceRNA sponge in GC is provided. Additional sequencing datasets from the GEO and Cancer Genome Atlas (TCGA) databases are downloaded and combined with this group's previous sequencing data to perform a joint analysis to expand the sample size. This study also constructs the ceRNA networks, performs the functional analysis, and verifies the hsa_circ_0072309 expression in GC tissues and cell lines. This paper also investigates the anti-cancer ability of hsa_circ_0072309 through gain- and loss-of-function experiments and identifies the binding site between circRNA and miRNA in vitro. To further explore its clinical value, this study investigates the relationship between the expression of hsa_circ_0072309 and the clinical characteristics of patients, including gender, age, tumor size, degree of differentiation, infiltration depth, vascular invasion, and lymph node metastasis (LNM). Additionally, the expression pattern and survival prognosis of its downstream targeted miRNAs and mRNAs in the TCGA database and the correlation between the DEMs and immune infiltration are studied.

2. Materials and methods

2.1. Data preparing

The TCGA transcriptional data, survival data, miRNA expression profile data, and clinical data of GC (stomach adenocarcinoma [STAD]) were downloaded with the UCSC Xena browser (http://xena.ucsc.edu/) [12]. The microarray data from two gene expression profile datasets (GSE83521 and GSE100170) were downloaded from the GEO database; both of them were obtained from the GPL19978 and GPL23259 platforms.

A total of 34 patients with GC receiving radical gastrectomy at Zhejiang Provincial People's Hospital between October 2017 to December 2018 were enrolled in this study; they had never received radiotherapy, chemotherapy, or targeted therapy before surgery. All the postoperative specimens were diagnosed as GC by pathologists. This study obtained approval from the Research Ethics Committee of Zhejiang Provincial People's Hospital, Hangzhou Medical College (ethics no. 2020QT084).

Human gastric epithelium cells (GES1) and human GC cells (MNK-45 and HGC-27) were procured from the Shanghai Cell Bank of Chinese Academy of Sciences (Cell Bank of the Chinese Academy of Sciences, Shanghai, China), and human gastric adenocarcinoma (AGS) cells were obtained from the American Tissue Culture Collection (Rockville, MD, USA). Both GES1 and HGC-27 were cultured in dulbecco's modified eagle medium (DMEM), AGS was cultured in F-12K, and MKN-45 was cultured in RPMI-1640. The culture medium was supplemented with 1% penicillin/streptomycin (Sigma, St. Louis, MO, USA) and 10% fetal bovine serum (FBS) (Hyclone, Logan, UT, USA). All cells were incubated at 37 °C in a humidified 5% CO_2 atmosphere.

2.2. Differentially expressed circRNAs in GC

The limma [13] package was used to read the original data of the two chips and to annotate their corresponding data to the platform information. The differentially expressed circRNAs (DECs) from the three datasets were screened using the limma linear model fitting and empirical Bayesian methods; $P < 0.05$ and logFC >1 were the thresholds for the up-regulated circRNA (UR-circRNA), and $P < 0.05$ and log FC < -1 were the thresholds for the down-regulated circRNA (DR-circRNA). After this was determined, the common DECs of the three datasets were screened as a collection of DECs.

2.3. The expression pattern of hsa_circ_0072309

The circRNA expression profile data of STAD in this study's spectrum chips were sorted out to explore the differential expression pattern of hsa_circ_0072309 in cancer (cancer group) and paracancerous tissues (normal group), and the structural position of the DECs was studied.

2.4. Prediction of the miRNAs regulated by DECs

A prediction of the miRNAs came from four authoritative databases: the cancer specific circRNA database (CSCD) (http://gb.whu.edu.cn/CSCD/) [14], the circbank (http://www.circbank.cn/) [15] database, the TargetScan [16] database, and the CircFunBase (http://bis.zju.edu.cn/CircFunBaseBlast/) [17] database. The DEC and differentially expressed miRNA (DEMI) pairs were visualized by Cytoscape software [18].

2.5. Expression profile analysis of target miRNAs

The miRNA expression profile of GC, downloaded from the TCGA database, was preprocessed before undergoing quantitative analysis. Fragments per kilobase of exon models per million mapped fragments (FPKM) was converted to trans per kilobase of exon models per million mapped reads (TPM), in which the TPM value was calculated as the transcript read per thousand base transcripts per million mappings. The TPM value was used to measure the expression of miRNAs more accurately. Then, the data was standardized by log2 transformation to make the data conform to the requirements of normal distribution. Next, the expression value of the miRNAs regulated by hsa_circ_0072309 was extracted to analyze the expression pattern of the miRNA in the cancer and normal groups.

2.6. Survival analysis of high- and low-risk target miRNAs in STAD

The median value of the TCGA TPM expression data of the STAD miRNAs in the tissues was used as the threshold to distinguish between the high-risk (HR) and low-risk (LR) groups. The target miRNAs above the median were sorted into the HR group, and the rest were sorted into the LR group. Moreover, the Kaplan–Meier (KM) survival curve was generated by the R language survival rates, survminer package, and survfit function. In the logrank test, $P < 0.05$ was considered significant in the survival rate differences between the HR and LR groups.

2.7. Prediction of the downstream target genes of the miRNAs regulated by hsa_circ_0072309

The mRNA genes were predicted from four authoritative databases: TargetScan (http://www.targetscan.org/vert_72/), miRTarBase (https://mirtarbase.cuhk.edu.cn/miRTarBase/miRTarBase_2019/php/index.php) [19], miRBase (http://www.mirbase.org/) [20], and miRanda (http://cbio.mskcc.org/miRNA2003/miranda.html) [21]. Only the mRNAs that existed in at least two of the databases were screened out to build the miRNA–mRNA networks visualized with Cytoscape [18] software.

2.8. Differentially expressed genes and receiver operating characteristic analysis

Among the target genes obtained above, the limma package was used to screen out the DEMs with a threshold of an adjusted $P < 0.05$ and $|\log FC| > 2$ (cancer group and normal group). For the survival analysis, the median expression value of the DEMs was taken as the cut-off value, and a KM curve followed by a logrank test was plotted. The statistical significance level was set at $P < 0.05$.

2.9. Gene ontology and Kyoto encyclopedia of genes and genomes enrichment analysis

The DAVID (https://david.ncifcrf.gov/) [22], an online website enrichment tool, was used to perform the Gene Ontology (GO) and Kyoto Encyclopedia of Genes and Genomes (KEGG) analysis with the statistical significance set as an adjusted $P < 0.05$. The enrichment results were visualized by the R language ggplot2 package, while the enrichment results of the KEGG analysis were visualized with the Cytoscape ClueGO [23] plug-in.

2.10. Correlation analysis of immune cell infiltration

CIBERSORT (https://cibersort.stanford.edu/) [24] is a deconvolution algorithm of transcriptome expression matrix based on the

principle of linear support vector regression to estimate the composition and abundance of immune cells in mixed cells. Timer [25] is a database that integrates a variety of immune cell infiltration algorithms.

To study the correlation between the genes of interest and immune cells, a scatter diagram was generated to demonstrate the correlation using the Timer database and CIBERSORT algorithm. The Spelman method was used for calculating the correlation coefficient between immune cell infiltration and gene expression and its statistical test P value. A significant correlation between gene expression and immune cells was established when $P < 0.05$.

2.11. Real-time quantitative polymerase chain reaction

The total RNA of the tissues and cells was extracted with TRIzol Reagent (Invitrogen, USA) and quantified using the NanoDrop ND2000 (Thermo Fisher Scientific, USA). The complementary DNA (cDNA) was synthesized with the iScript cDNA synthesis kit (Bio-Rad, Hercules, CA, USA). The expression level of the circRNA was analyzed by real-time quantitative polymerase chain reaction (RT-qPCR) using SYBR Green Premix Ex TaqTM (Takara, Japan). The primers for used for the circRNA and glyceraldehyde-3-phosphate dehydrogenase (GAPDH) are shown in Table 1. The RT-qPCR data were analyzed by the ΔCt and $2^{-\Delta\Delta Ct}$ methods, whose values represented the sample's expression and the relative expression, respectively [26]. The experimental results were presented as the mean ± standard deviation. Each assay was performed in triplicate.

2.12. Small interfering RNA transfection

Small interfering RNAs (siRNAs) targeting hsa_circ_0072309 (Guangzhou RiboBio Co., Ltd.) (sequences are shown in Table 1) were used to knockdown the expression of hsa_circ_0072309. Control: normal culture of AGS or MKN-45 cells; SiRNA scrambled: AGS or MKN-45 cells transfected with siRNA scrambled; SiRNA-circ0072309: AGS or MKN-45 cells transfected with siRNA-circ0072309; Lipofectamine® RNAiMAX (13778030) (Thermo Fisher Scientific, Pittsburgh, PA, USA) was used for the transfection, as per the manufacturer's protocol.

2.13. Overexpression of plasmids and stable cells transfection

The plasmid vector was constructed by GenePharma (Shanghai, GenePharma, Co., Ltd.) and packed with lentivirus by BIORN (BIORN lifescience Co., Ltd.) for the overexpression study. Control: HGC-27 or MKN-45 cells were cultured normally. Oe vector: HGC-27 or MKN-45 cells transfected with oe-vector lentivirus plasmid. Oe-circ0072309: HGC-27 or MKN-45 cells transfected with oe-circ0072309 lentivirus plasmid.the stable cells were selected with 200 μg/mL of Puromycin.

2.14. Cell viability assay

Cell Counting Kit-8 (CCK-8) (Beyotime, Shanghai, China) assays were performed to measure the proliferation of the GC cells transfected with oe-vector or oe-circ_0072309/siRNA-scrambled or siRNA-circ0072309. The cells were collected by centrifugation and inoculated into a 96-well plate at the density of 1×10^4/well. There were three multiple holes for each experimental group. Ten μm of CCK-8 agent was added to each well at 24 h. After incubation for 2 h at 37 °C, the optical density of each well was measured at 450 nm. All experiments were repeated three times and were performed in triplicate.

Table 1
Primers sequences used in RT-qPCR/qPCR and plasmids sequences of siRNAs/negative control (siRNA-scrambled) and miRNA mimics/mimics NC.

	Sequence (5′-3′)
hsa_circ_0072309-Forward	CTCAACCTCTACATTATACCTAA
hsa_circ_0072309-Reverse	CCTAGGGACCCTGGTATGGATC
GAPDH-Forward	GCACCGTCAAGGCTGAGAAC
	TGGTGAAGACGCCAGTGGA
GAPDH- Reverse hsa-miR-34a-3p-Forward	GGCGGCAATCAGCAAGTATAC
hsa-miR-34a-3p-Reverse	CAGTGCAGGGTCCGAGGTAT
hsa-miR-330-5p-Forward	TCTCTGGGCCTGTGTCTTAGGC
hsa-miR-330-5p-Reverse	CTAAGACACAGCCCAGAGATT
SiRNA-scrambled	TTCTCCGAACGTGTCACGT
siRNA-circ0072309#1	GCCCTGAGCAGAAACATAA
siRNA-circ0072309#2	GAGCAGAAACATAAGCTGT
siRNA-circ0072309#3	GCAGAAACATAAGCTGTGG
mimics NC	UUUGUACUACACAAAAGUACUG
hsa-miR-34a-3p mimics	CAAUCAGCAAGUAUACUGCCCU
hsa-miR-330-5p mimics	UCUCUGGGCCUGUGUCUUAGGC
hsa-miR-148a-3p mimics	UCAGUGCACUACAGAACUUUGU
hsa-miR-331-5p mimics	CUAGGUAUGGUCCCAGGGAUCC

2.15. Colony formation assay

The GC cells were inoculated into a 6-well plate at the density of 1×10^3/well. After incubation for 1 week, the cells were fixed with 4% paraformaldehyde for 30 min and stained with 1% crystal violet (KeyGEN Biotech, NanJing, China) for 15–20 min. The colonies were imaged and counted for statistical analysis. Each assay was performed in triplicate.

2.16. Scratch wound assay

The cells were treated with mitomycin (5 μg/ml) for 1 h when they reached the confluence of 80%–90% in the 6-well plates; then, they were scratched with a 10-μm micropipette tip. Images were taken at the start and at 24 h and were analyzed by Image-J software. Each group was repeated in triplicate independently. Each assay was performed in triplicate.

2.17. Transwell invasion and migration assay

A cell (2.5×10^5/ml) suspension (100 μm of serum-free medium) was added into the upper chamber of a 24-well transwell with Matrigel (BD Bioscience, USA) for the invasion assay or without Matrigel for the migration assay. Then, 600 μm of medium (with 10% FBS) was added to the lower chamber. After incubation for 24 (migration) or 48 (invasion) h, the transwell assay was fixed and stained with 4% formaldehyde and 1% crystal violet, respectively. Finally, the upper chamber was placed upward onto slides to count the cells passing through the chamber with a microscope. The counting field was randomly selected. Each assay was performed in triplicate.

2.18. Dual-luciferase reporter assay

Empty plasmid hsa_circ_0072309-WT, hsa_circ_0072309-MUT#1, or hsa_circ_0072309-MUT#2, or hsa-miRNA mimics (hsa-miR-330-5p and hsa-miR-34a-3p) or hsa-miRNA mimics-NC (hsa-miR-330-5p and hsa-miR-34a-3p), were constructed by BIORN (BIORN lifescience Co., Ltd.) and transfected into the AGS cells. Circ0072309-WT + mimics NC group: AGS cells transfected with circ0072309-WT luciferase reporter gene plasmid and mimics NC plasmid.Circ0072309-WT + hsa-miR-34a-3p mimics group: AGS cells transfected with circ0072309-WT luciferase reporter gene plasmid and+hsa-miR-34a-3p mimics plasmid.Circ0072309-MUT # 1+mimics NC group: AGS cells transfected with circ0072309-MUT # 1 (the binding site mutation of circ0072309 and hsa-miR-34a-3p) luciferase reporter gene plasmid and mimics NC plasmid.Circ0072309-MUT # 1+hsa-miR-34a-3p mimics group: AGS cells transfected with circ0072309-MUT # 1 (circ0072309 and hsa-miR-34a-3p binding site mutation) luciferase reporter gene plasmid and hsa-miR-34a-3p mimics plasmid.Circ0072309-WT + hsa-miR-330-5p mimics group: AGS cells transfected with circ0072309-WT luciferase reporter gene plasmid and hsa-miR-330-5p mimics plasmid.Circ0072309-MUT # 2+mimics NC group: AGS cells transfected with circ0072309-MUT # 2 (circ0072309 and hsa-miR-330-5p binding site mutation) luciferase reporter gene plasmid and mimics NC plasmid. Circ0072309-MUT # 2+hsa-miR-330-5p mimics group: AGS cells transfected with circ0072309-MUT # 2 (mutation of the binding site of circ0072309 and hsa-miR-330-5p) luciferase reporter gene plasmid and hsa-miR-330-5p mimics plasmid.The sequences for the miRNAs are shown in Table 2. A dual-luciferase reporter assay kit (Beyotime, Shanghai, China) was used to measure the luciferase activity, as per the manufacturer's protocol. Each assay was performed in triplicate.

2.19. Argonaute2-ribonucleoprotein immunoprecipitation assay

An Argonaute2-ribonucleoprotein immunoprecipitation (AGO2-RIP) assay was performed on the AGS cells using an RIP kit (RIP-

Table 2
Relationship between the expression of hsa_circ_0072309 in gastric cancer and clinical features.

Clinical features	n (%)	ΔCt value	t	P
Gender				
Male	26 (76.5)	24.95 ± 1.44	0.7727	0.4455
Female	8 (23.5)	24.49 ± 1.55		
Age, years				
<60	10 (29.4)	24.21 ± 1.20	1.670	0.1046
≥60	24 (70.6)	25.10 ± 1.49		
Tumor (cm)				
<5 cm	20 (58.8)	24.19 ± 1.28	3.704	0.0008***
≥5 cm	14 (41.2)	25.78 ± 1.17		
Invasion depth				
Ta-T2	14 (41.2)	24.36 ± 1.33	1.648	0.1092
T3-T4	20 (58.8)	25.18 ± 1.48		
vascular invasion				
NO	13 (38.2)	23.579 ± 2.768	3.129	0.0037**
Yes	21 (61.8)	25.210 ± 2.005		
Lymph node metastasis				
N0	13 (38.2)	24.10 ± 1.12	2.535	0.0163*
N1-N3	21 (61.8)	25.30 ± 1.47		

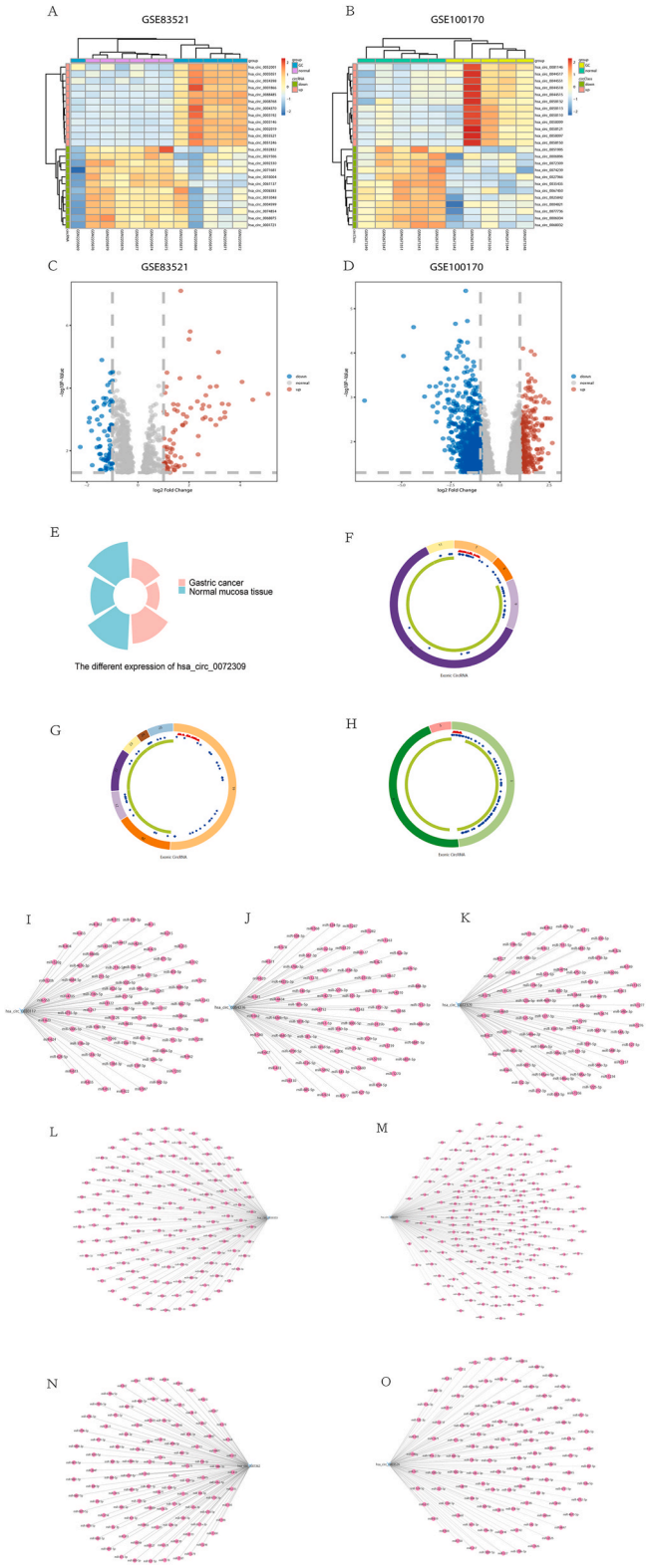

Fig. 1. Expression pattern of differentially expressed circular RNAs (DECs). (A) Heatmap of DECs in the GSE83521 dataset. (B) Heatmap of DECs the in GSE100170 dataset. (C) Volcano plot of DECs in the GSE83521 dataset. (D) Volcano plot of DECs in the GSE100170 dataset. (E) Differential expression pattern of hsa_circ_0072309 in this research group's sequencing chip. (F) The structural diagram of hsa_circ_0003526. (G) The structural diagram of hsa_circ_0006039. (H) The structural diagram of hsa_circ_0039353. The red, blue, and green regions inside the circular RNA molecular

structure represent a microRNA response element), a RNA binding protein, and an open reading frame, respectively. Networks of 7 common DECs interacting with miRNAs in the four databases (the cancer specific circRNA database, TargetScan, cirbank, and cirFunBase): (I) hsa_circ_0030117, (J) hsa_circ_0064336, (K) hsa_circ_0072309, (L) hsa_circ_0039353, (M) hsa_circ_0006039, (N) hsa_circ_0001362, and (O) hsa_circ_0003526.

12RXN) (Sigma, St. Louis, MO, USA). The lysed AGS cells were incubated with magnetic beads coated with AGO2 antibodies (Cell Signaling Technology, Boston, USA) or immunoglobulin G, per the manufacturer's instruction. The abundance of hsa_circ_0072309, hsa-miR-34a-3p, and hsa-miR-330-5p in the precipitates were determined by RT-qPCR and gel electrophoresis. The primers used are shown in Table 1. Each assay was performed in triplicate.

2.20. Statistical analysis

All data analyses in this paper were performed using R software (version 3.6.2) and graphpad software (version 8.3). All the in vitro data were presented as the mean ± standard deviation, and the statistical differences between the experimental group and the control group were calculated by a one-way analysis of variance and Tukey's test ($P < 0.05$ was considered statistically significant).

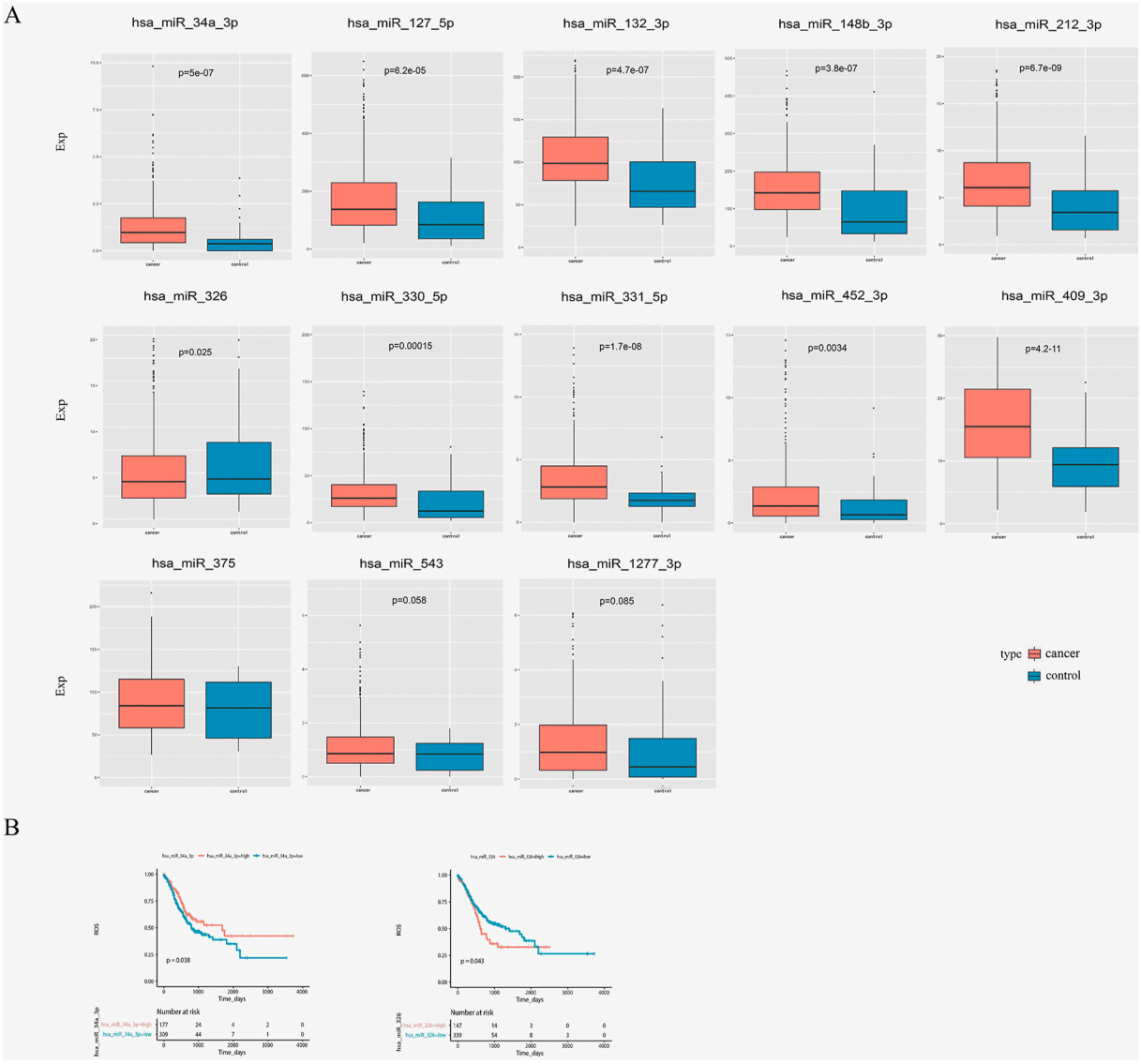

Fig. 2. Expression pattern and prognosis of 13 differentially expressed micro RNAs (DEMIs) in cancerous and paracancerous tissues. (A) Expression pattern of 13 DEMIs in gastric cancer and normal tissues (control group). (B) Survival curves of two screened DEMIs whose *P* values were less than 0.05 by a logrank test.

3. Results

3.1. Identification of DECs

The differential expression analysis of the three databases (GSE100170, GSE83521, and TCGA) was performed by the limma package. The results revealed 124 circRNA (103 DR-circRNA and 21 UR-circRNA) were differentially expressed in the GSE100170 database (Fig. 1A and B), 149 circRNA (70 DR-circRNA and 79 UR-circRNA) were differentially expressed in the GSE83521 database (Fig. 1C and D), and 248 circRNA (114 DR-circRNA and 134 UR-circRNA) were differentially expressed in the TCGA database. Using the selection criteria of $P < 0.05$ and $|\log FC| > 1$, a total of seven DECs were screened: hsa_circ_0030117, hsa_circ_0006039, hsa_circ_0064336, hsa_circ_0039353, hsa_circ_0003526, hsa_circ_0001362, and hsa_circ_0072309. Furthermore, significantly different expression patterns of DECs were observed between the cancer and the normal group ($P < 0.05$).

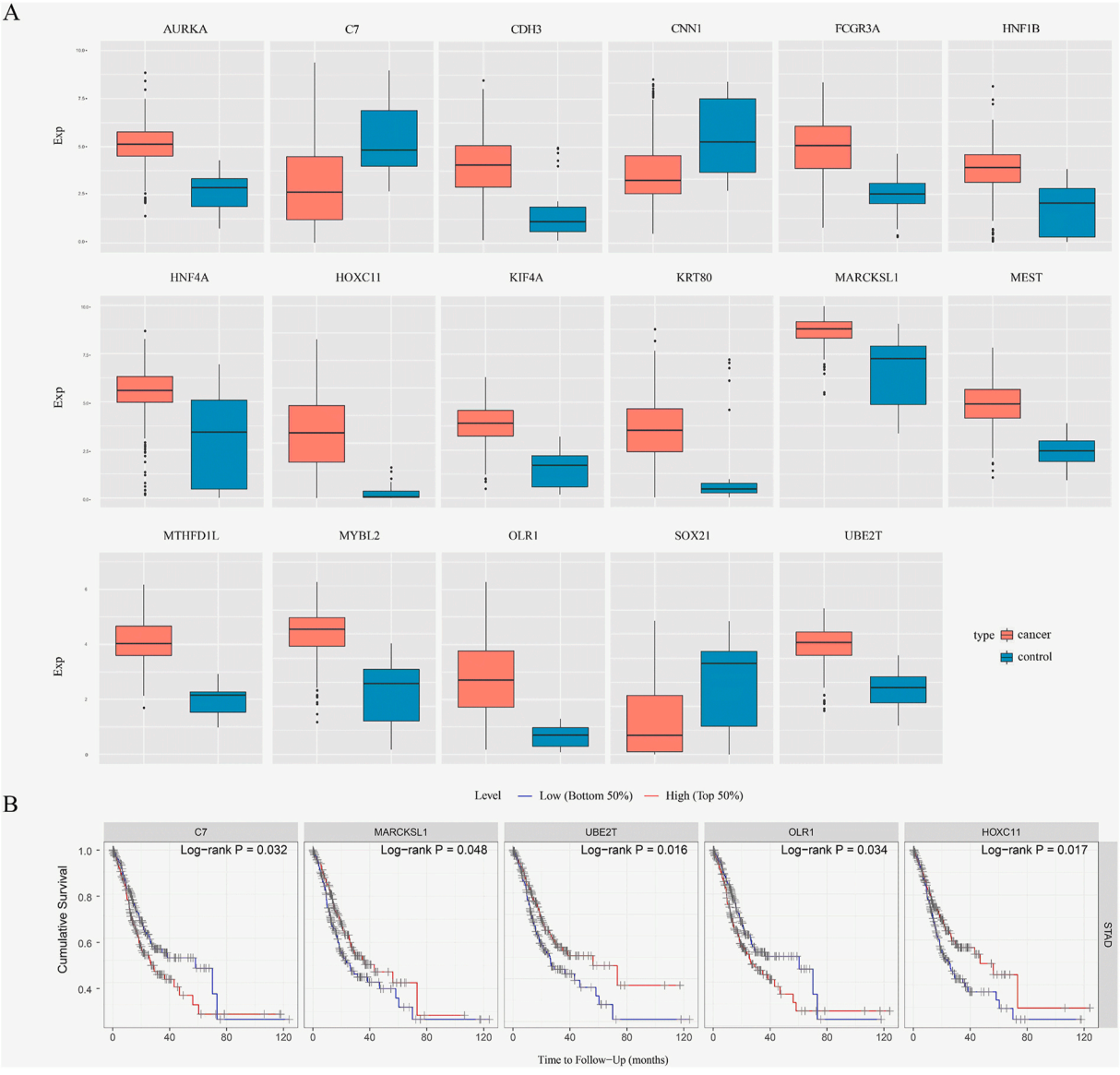

Fig. 3. Expression pattern and prognosis of 17 differentially expressed messenger RNAs (DEMs) in cancerous and normal tissues (control group). (A) Expression pattern of 17 DEMs in gastric cancer and normal tissues (control group). (B) Survival curves of five screened DEMs whose *P* values were less than 0.05 by a logrank test.

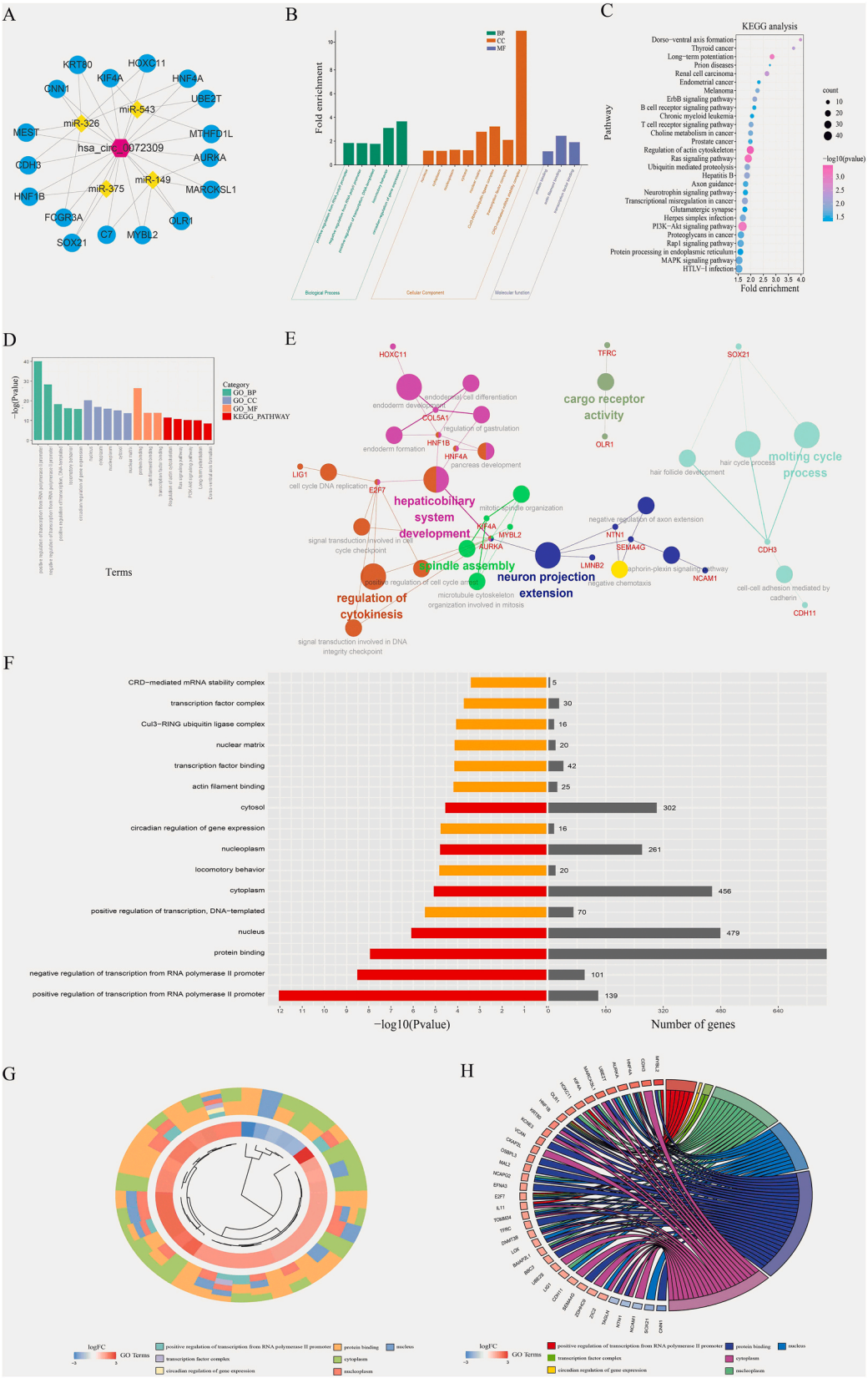

(caption on next page)

Fig. 4. Competing endogenous RNA (ceRNA) network and enrichment analysis of target genes. (A) CeRNA network of has_circ_0072309. (B) Histogram of the Gene Ontology enrichment analysis. (C) Bubble plots of the Kyoto Encyclopedia of Genes and Genomes (KEGG) enrichment analysis. (D) Histogram of molecular functions (MF), cellular components (CC), (biological procese) BP, and KEGG pathway enrichment analyses. (E) Enrichment results of the KEGG pathway. (F) The GO enrichment analysis results, where the enriched GO terms are on the left; the red concentration represents the significant degree of enrichment, and the gray column on the right represents the number of genes enriched by the GO term. (G) Heat map of the GO enrichment results of the seven genes of interest. (H) The GO enrichment results and chord plot of the seven genes of interest.

3.2. The expression pattern of DECs

The differential expression of hsa_circ_0072309 in the cancer and the normal tissues in this study's microarray are presented in Fig. 1E. Existing DECs were selected from the CSCD database, searched in the "cirBase," and the location information of three down-regulated DECs (hsa_circ_0003526, hsa_circ_0006039, and hsa_circ_0039353) were discovered. The structural patterns of these three DECs are shown in Fig. 1F–H.

3.3. Prediction of the miRNAs targeted by the DECs

The target miRNAs of the seven DECs were predicted with CSCD, TargetScan, cirbank, and cirFunBase. The circRNA and miRNA regulatory networks are shown in Fig. 1I–O; hsa_circ_0072309 is visible in Fig. 1K.

3.4. Expression pattern analysis of the target miRNAs

According to method above, the miRNAs predicted by hsa_circ_0072309 were extracted and 13 DEMIs were obtained. Ten of these miRNAs exhibited differential expression patterns in cancer and the normal tissues (Fig. 2A). Among these DEMIs, hsa_miR-34a-3p, hsa_miR-127-5p, hsa_miR-132-3p, hsa_miR-148b-3p, hsa_miR212-3p, hsa_miR-330-5p, hsa_miR-331-5p, hsa_miR-452-3p, and hsa_miR-409-3p were up-regulated ($P = 5.0 \times 10^{-7}$, 6.2×10^{-5}, 4.7×10^{-7}, 3.8×10^{-7}, 6.7×10^{-9}, 0.00015, 1.7×10^{-8}, 0.0034 and 4.2×10^{-11}, respectively), while hsa_miR-326 was down-regulated ($P = 0.025$).

3.5. Survival analysis of the high- and low-risk target miRNAs in STAD

To explore the prognostic efficacy of these 13 DEMIs, the clinical data of GC from the TCGA database was downloaded. A logrank test was performed, after which the miRNAs with *P*-value of <0.05 were selected to plot a KM survival curve (Fig. 2B, supplementary file: Fig. 1). A high expression of hsa_miR-34a-3p showed better survival outcomes ($P = 0.034$).

3.6. Prediction of downstream mRNAs of miRNAs targeted by hsa_circ_0072309

The prediction of the downstream target mRNAs came from four authoritative databases: TargetScan, miRanda, miRTarBase, and miRBase. Only the mRNAs in at least two databases were screened, and 69,695 miRNAs–mRNAs pairs were identified. By taking the intersection of these mRNAs and the TCGA data, a total of 1460 mRNAs were screened (supplementary file: Fig. 2).

3.7. DEGs and ROC analysis

The limma package was used to screen the 1460 DEMs with an false discovery rate (FDR) < 0.05 and a $|\log FC| > 2$ as the threshold, and 17 DEMs were finally obtained. Combining the expression of the genes and the survival data in the TCGA database, the expression patterns and prognostic efficacy of those 17 DEMs were analyzed. The survival analysis was measured by a logrank test, and $P < 0.05$ was set as statistically significant. As is shown in Fig. 3A, all the DEMs were up-regulated except for three genes: complement component 7 (C7) ($P = 1.4 \times 10^{-7}$), CNN1 ($P = 7.1 \times 10-^{7}$), and SOX21 ($P = 1.7 \times 10^{-6}$). The survival analysis revealed that only 5 of the 17 genes, C7 ($P = 0.032$), MARCKSL1 ($P = 0.048$), UBE2T ($P = 0.016$), OLR1 ($P = 0.034$), and HOXC11 ($P = 0.017$), showed significant differences in the high- and low-risk groups (Fig. 3B).

3.8. GO and KEGG enrichment analyses

The ceRNA network diagram is shown in Fig. 4A. The GO and KEGG enrichment analyses were performed on all 17 DEMs; the results were organized into functional pathways using the DAVID web tools and visualized with R package ggplot2 software. The GO annotation revealed that related biological processes included the following: positive regulation of transcription from RNA polyII promoter, response to glucose, and anterior/posterior pattern specification. Interestingly, the circadian regulation of gene expression was also among the listed enriched terms, and the related cellular components included the nucleus, cytoplasm, and nucleoplasm. The enriched molecular functions were protein binding, actin filament binding, and transcription factor binding. The PI3K-Akt and Ras signal pathways were the most significantly enriched pathways (Fig. 4B–F; supplementary file: Tables 1 and 2). In addition, seven GO enrichment results of interest were selected to generate a heat map and chord plot (Fig. 4G and H). The enriched terms mentioned above had a substantial impact on transcription and cell division; the pathways related to PI3K-Akt, Ras, and MAPK suggest the critical

roles of these DEMs in GC tumorigenesis.

3.9. Correlation analysis of immune cell infiltration

A correlation analysis was performed between the six genes of interest (AURKA, C7, CDH3, CNN1, HNF1B, and HOXC11) and the immune infiltrates using the online tools CIBERSOFT (https://cibersort.stanford.edu/) and Timer (https://cistrome.shinyapps.io/timer/). The results are displayed on scatter plots (Fig. 5). The correlation between the degree of immune infiltrates and gene expressions as well as the *P* value were calculated by the Spelman's coefficient method. AURKA was negatively correlated with B cells, $CD8^+$ cells, $CD4^+$ cells, macrophages, neutrophils, and dendritic cells ($P = 1.28 \times 10^{-4}$, 1.99×10^{-6}, 3.69×10^{-7}, 4.02×10^{-15}, 8.28×10^{-5}, and 8.4×10^{-9}); C7 was positively correlated with B cells, $CD8^+$ cells, $CD4^+$ cells, macrophage, neutrophils, and dendritic cells ($P = 1.89 \times 10^{-4}$, 1.14×10^{-6}, 1.77×10^{-29}, 7.49×10^{-39}, 3.14×10^{-5}, and 9.31×10^{-18}); CDH3 was negatively correlated with $CD8^+$ cells, $CD4^+$ cells, macrophages, and dendritic cells ($P = 2.19 \times 10^{-3}$, 3.62×10^{-4}, 4.12×10^{-4}, and 1.53×10^{-2}); HNF4A and HOXC11 were negatively correlated with $CD8^+$ cells, macrophages, neutrophils, and dendritic cells ($P = 3.42 \times 10^{-7}$, 1.47×10^{-9}, 4.97×10^{-8}, and 3.55×10^{-9} and $P = 3.54 \times 10^{-6}$, 1.17×10^{-5}, 2.57×10^{-5}, and 7.29×10^{-8}, respectively); and HNF1B was negatively correlated with macrophages, neutrophils, and dendritic cells ($P = 4.41 \times 10^{-2}$, 1.39×10^{-2}, and 3.35×10^{-3}).

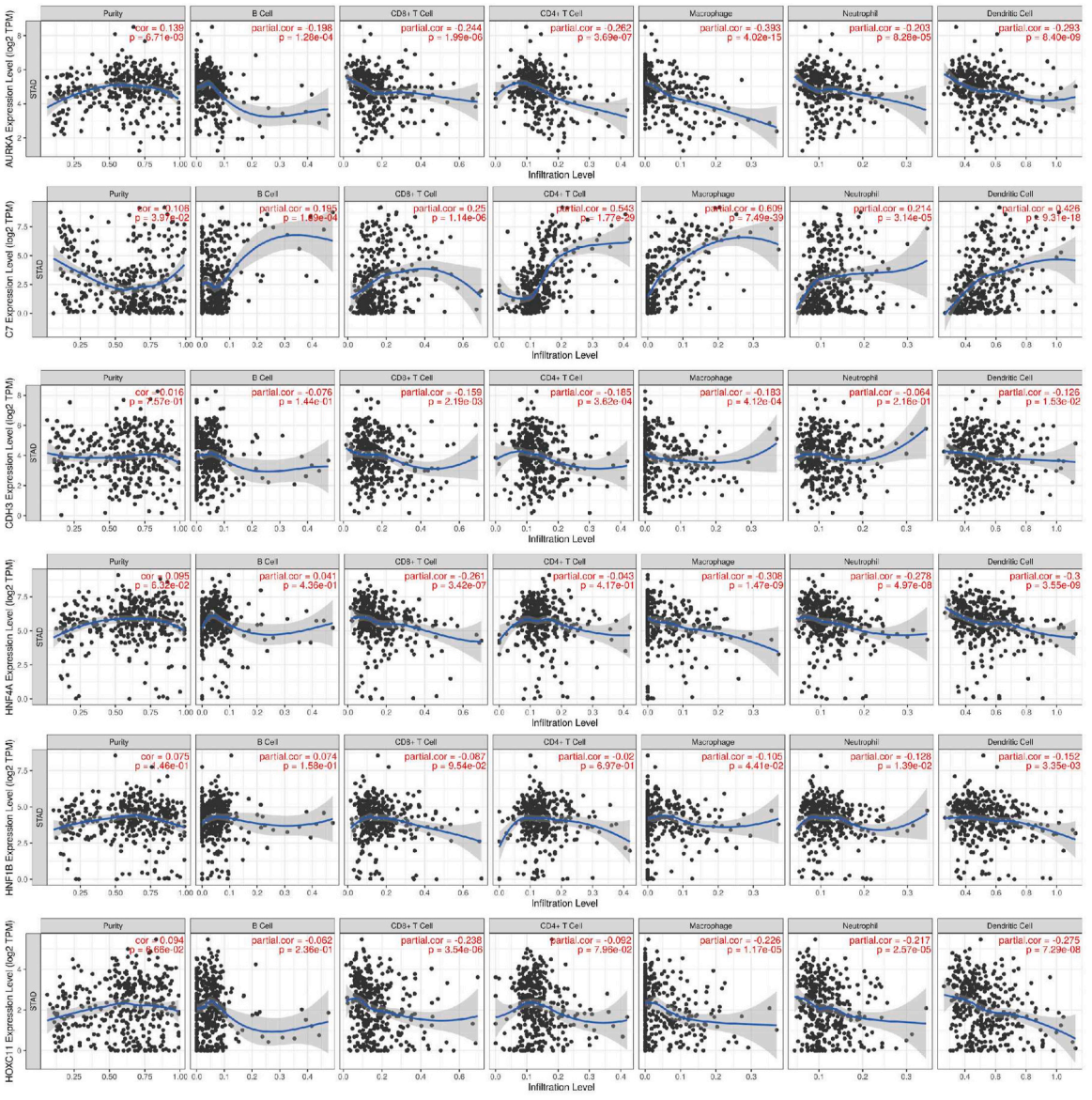

Fig. 5. Scatter plots of the relationship between the expression of the target genes AURKA, C7, CDH3, CNN1, HNF1B, and HOXC11 and the immune infiltration.

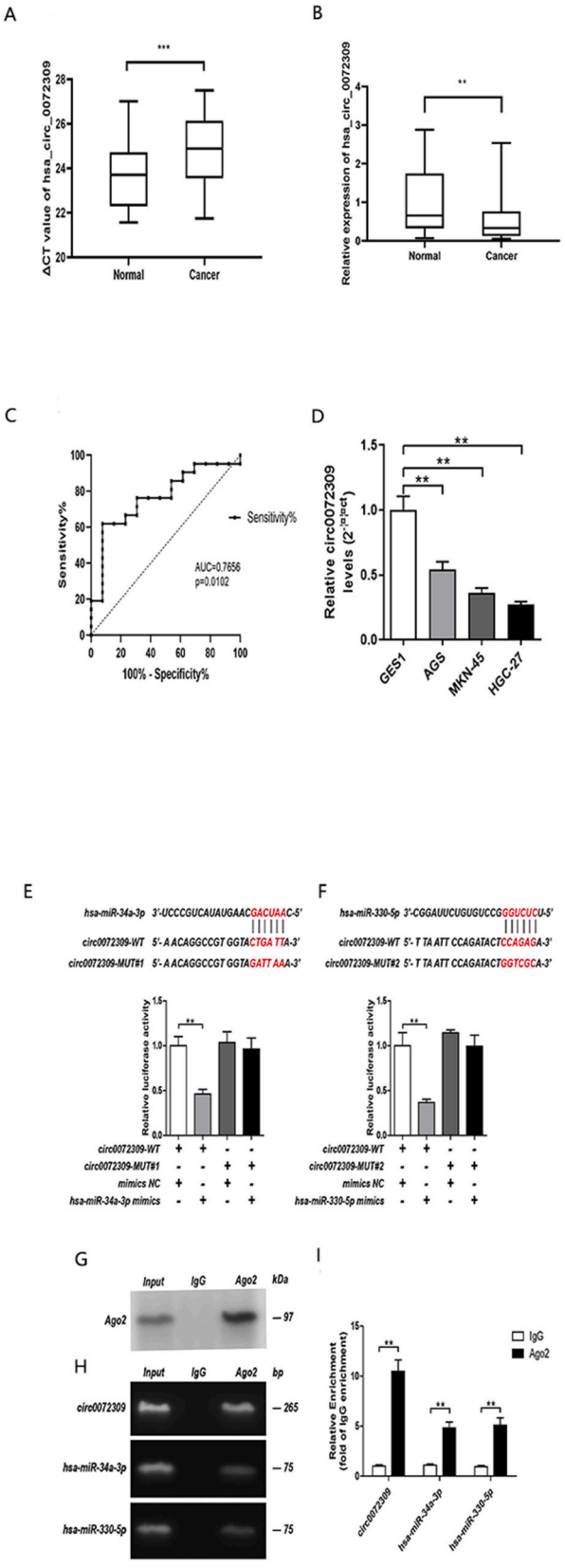

(caption on next page)

Fig. 6. Hsa_circ_0072309 was down-regulated in in vivo (A–C) and in vitro (D) assays and could bind to hsa-miR-34a-3p and hsa-miR-330-5p. (E) Hsa-miR-34a-3p could bind to hsa_circ_0072309-WT at hsa_circ_0072309 (248-CTGATT-256). (F) Hsa-miR-330-5p could bind to hsa_circ_0072309-WT at hsa_circ_0072309 (433-CCAGAG-440). (G–I) The argonaute2-ribonucleoprotein immunoprecipitation assay revealed that both hsa-miR-34a-3p and hsa-miR-330-5p may bind to hsa_circ_0072309. All results are presented as the mean ± standard deviation for three individual experiments. $^{*}P < 0.05$, $^{**}P < 0.01$.

3.10. Hsa _circ_0072309 was downregulated in vivo and in vitro

Hsa_circ_0072309 expression was validated in 34 paired GC tissues and non-cancerous tissues (normol tissues) and GC cell lines by RT-qPCR, and the results revealed a significant down-regulated hsa_circ_0072309 in GC tissues and cell lines (Fig. 6A–D). Furthermore, in vitro experiments revealed that among the GC cells, the topmost expression level of hsa_circ_0072309 was in the AGS cells while the lowest was in the HGC-27 cells.

3.11. Associations between hsa_circ_0072309 expression level and clinical characteristics in GC

The relationship between the hsa_circ_0072309 expression level and the clinical features of patients with GC were further investigated. The hsa_circ_0072309 expression level was associated with tumor size ($P = 0.0008$), vascular invasion ($P = 0.0037$), and LNM ($P = 0.0163$) (Table 2). Interestingly, most of these GC patients were over 60 years old (70.6%), and most of them were male (76.5%). However, no correlation was found between the hsa_circ_0072309 expression level and the patient's gender, age, and tumor invasion depth ($P < 0.05$). The ROC curve was plotted to further explore the clinical significance of LNM in GC. The area under the curve was 0.7656 (sensitivity was 61.9% and specificity was 92.31%), with a cut-off value of ΔCT at 25.34.

3.12. Hsa_circ_0072309 could bind to has-miR-34a-3p and has-miR-330-5p

According to the result of "Survival Analysis of the high- and low-risk target miRNAs in STAD", hsa-miR-34a-3p was selected, and three miRNAs (hsa-miR-330-5p, hsa-miR-148b-3p, and hsa-miR-331-5p) were randomly selected that were highly expressed in GC for the interaction experiments. As is demonstrated in Fig. 6E and F, hsa-miR-34a-3p and hsa-miR-330-5p significantly reduced the luciferase activity of the AGS cells transfected with hsa_circ_0072309-WT but not hsa_circ_0072309-MUT#1 (mutated sites at 248-CTGATT-256) or hsa_circ_0072309-MUT#2 (mutated sites at 433-CCAGAG-440), revealing that hsa-miR-34a-3p and hsa-miR-330-5p may directly bind to hsa_circ_0072309 at the mutated sites. The AGO2-RIP assay showed that the abundances of hsa_circ_0072309, hsa-miR-34a-3p, and hsa-miR-330-5p in the precipitates were significantly increased, revealing that hsa-miR-34a-3p and hsa-miR-330-5p may bind to hsa_circ_0072309 (Fig. 6G–I, supplementary file: Fig. 3).

3.13. Hsa_circ_0072309 overexpression suppressed whereas hsa_circ_0072309 knockdown promoted GC cells proliferation and migration in vitro

The HGC-27 and MKN-45 cell lines were selected for overexpression experiments. The results indicated that, compared with the cells transfected with oe-vector (control group), the cellular viability of the HGC-27 and MKN-45 cells transfected with oe-circ0072309 decreased significantly, as well as the invasion, migration, and colony formation abilities (Fig. 7).

The AGS and MKN-45 cell lines were selected for the knockdown experiments. Three siRNAs were designed to target hsa_circ_0072309, and siRNA-circ0072309#1 showed the best knockdown efficiency. As Fig. 8 demonstrates, the knockdown of hsa_circ_0072309 significantly increased the viability, invasion, migration, and colony formation abilities of the AGS and MKN-45 cells (transfected with siRNA-circ0072309#1).

4. Discussion

Gastric cancer, responsible for 8.2% of all cancer-related deaths in 2018, is still one of the deadliest cancers among gastrointestinal tumors, ranking third worldwide in terms of mortality [2]. Although significant progress has been made in the clinical diagnosis and treatment of GC in recent years, due to its atypical clinical presentation and the lack of specific diagnostic markers for early GC, 90% of diagnosed cases are at an advanced stage and tend to metastasize, leading to a poor five-year survival rate of less than 30% [27]. Therefore, it is vital to search for biomarkers related to the occurrence and prognosis of GC and develop new targets to improve the prognosis of diagnosed patients. With the advent of high-throughput sequencing technology, multiple circRNAs have been found to be dysregulated in GC, suggesting that they may contribute to its development and progression. Based on this research group's previous work on circRNAs and GC, additional chip data was downloaded from the GEO and TCGA databases and combined with this group's previous sequencing data. This study's purpose was to analyze hsa_circ_0072309 and its functions using bioinformatics methods, including differential expression analysis, GO and KEGG enrichment analyses, survival analysis on downstream miRNAs and mRNAs, and correlation analysis between DEGs and immune infiltration. Furthermore, the expression of hsa_circ_0072309 was validated in vivo and in vitro, functional experiments were performed on GC cell lines, the binding sites between hsa_circ_0072309 and its downstream miRNAs were identified, and the correlations between hsa_circ_0072309 expression and the clinical characteristics of patients diagnosed with GC were analyzed.

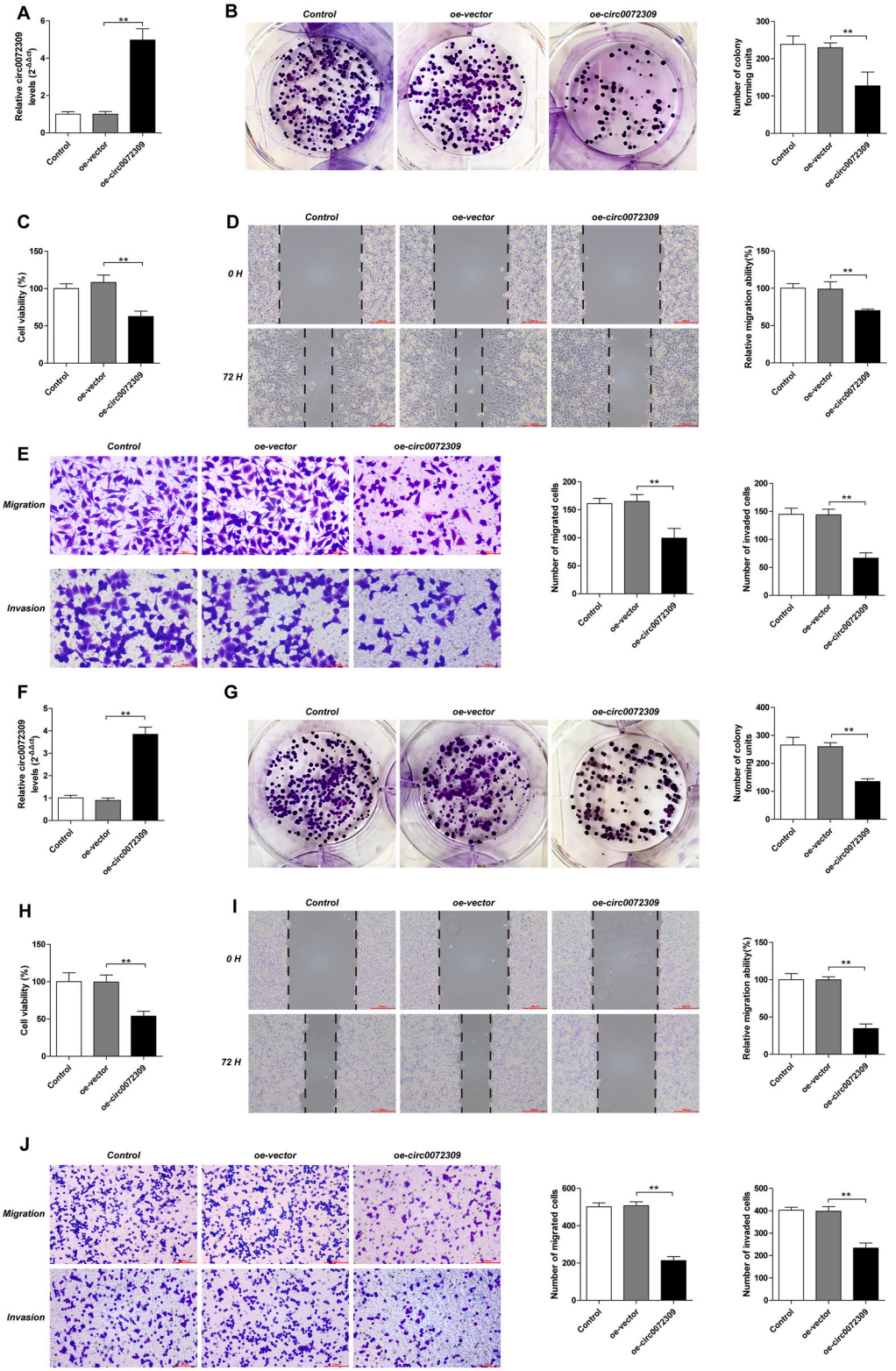

Fig. 7. Hsa_circ_0072309 overexpression suppressed the malignant phenotype of the HGC-27 (A–E) and MKN-45 (F–J) cell lines. Both cell lines were transfected with oe-vector or oe-circ0072309. The polymerase chain reaction showed their overexpression efficiency in the HGC-27 cells (A) and the MKN-45 cells (F). (B) The colony formation assay of hsa_circ_0072309 overexpression in the HGC-27 cells. (C) The cell viability of hsa_circ_0072309 overexpression in the HGC-27 cells was detected by Cell Counting Kit-8 (CCK-8). (D) The lateral migration ability of hsa_circ_0072309

overexpression in the HGC-27 cells was measured by wound healing assays. (E) The migration and invasion ability of hsa_circ_0072309 overexpression in the HGC-27 cells were analyzed by transwell assays. (G) The colony formation assay of hsa_circ_0072309 overexpression in the MKN-45 cells. (H) The cell viability of hsa_circ_0072309 overexpression in the MKN-45 cells was detected by CCK-8. (I) The lateral migration ability of hsa_circ_0072309 overexpression in the HGC-27 cells was measured by wound healing assays. (J) The migration and invasion abilities of hsa_circ_0072309 overexpression in the MKN-45 cells were analyzed by transwell assays. All results are presented as the mean ± standard deviation for three individual experiments. $^{*}P < 0.05$, $^{**}P < 0.01$.

Hsa_circ_0072309 was significantly downregulated in databases, including the GEO and TCGA databases as well as this group's chip data. Hsa_circ_0072309 down-regulation has previously been documented in breast cancer [28], hepatocellular carcinoma [29], and non-small cell lung cancer (NSCLC) [30]; these results were consistent with this study's analysis. Moreover, hsa_circ_0072309 was found to inhibit tumor progression by regulating targeted miRNA. It was suggested that hsa_circ_0072309 might have a similar function in GC as in the cancers mentioned above. To further investigate the functional effect of hsa_circ_0072309, in vitro experiments were performed; the results of which demonstrated that its overexpression suppressed GC cells, whereas its knockdown promoted the proliferation and migration of GC cells. Accordingly, the clinical relevance of the hsa_circ_0072309 expression level was further analyzed. The expression of hsa_circ_0072309 was associated with tumor size ($P = 0.0008$), vascular invasion ($P = 0.0037$), and LNM ($P = 0.00163$), suggesting that larger tumors, more severe invasion, and metastasis were related to the downregulation of hsa_circ_0072309 in GC. Indeed, it is widely acknowledged that most patients with malignant tumors die of metastasis [31]. In GC, lymph node metastasis is the most common way that the tumors spread [32] and is considered the most important factor in estimating the prognosis of patients with advanced GC [33]. Furthermore, the prediction of LNM in GC is key to adequate strategy management in the preoperative setting [34]. In this study, the ROC curve indicated that the expression value of hsa_circ_0072309 could be used to diagnose LNM in GC; therefore, hsa_circ_0072309 might be a potential biomarker for LNM detection in postoperative patients with GC. Thus, it is hypothesized that hsa_circ_0072309 may have protective effects and may inhibit invasion and metastasis in GC; it may also be a promising biomarker for the diagnosis and prediction of LNM in GC.

To further explore the functions of hsa_circ_0072309, GO and KEGG functional enrichment analyses were conducted on the DEGs. GO terms were related to the transcription, cell division, and circadian regulation of gene expression. Moreover, the most significantly enriched pathways were the PI3K-Akt, Ras, and MAPK pathways; these are classical pathways that have been documented to be correlated with tumorigenesis and development [35]. Interestingly, disturbances of the circadian clock have been reported to be involved in the development of various diseases, including cancer. In this regard, a large cohort study showed that an abnormal circadian rhythm resulting from late food intake might be related to carcinogenesis at different locations [36]. Over the years, epidemiological studies have shown that circadian rhythm disorders are associate with an increased risk of carcinomas, including prostate [37,38], colon, liver, pancreatic, breast, ovarian, and lung cancer [39]. Studies also indicated that a series of circadian clock-related genes, including CRY, PER, and BMAL1, could impact key pathways affecting the hallmarks of cancers, including cell-cycle control, DNA damage repair, apoptosis, and apoptosis metabolic regulation, alternating the cancer phenotypes [39]. Substantial evidence has suggested that BMAL1 plays a vital role in limiting tumorigenesis. Inhibiting BMAL1 expression has been shown to significantly increase prostate cancer, lung cancer, and glioma metastatic potential in vitro and in vivo, and the antitumor effect of BMAL1 may be modulated via the PI3K–AKT signal axis [40]. Based on the notion of circadian clock perturbation of cancer pathways, researchers put forward the concept of chronotherapy, which harnesses the natural rhythm and cycle of the body to treat diseases or disorders [41]. For instance, male colorectal cancer patients who received chronomodulated chemotherapy with oxaliplatin, 5-fluorouracil, and folinic acid experienced reduced toxicity and improved outcomes [42]. In a retrospective study, where 97 NSCLC patients underwent stereotactic radiosurgery for brain metastases, the morning group experienced significant improvements, including 3-month local control (97% versus 67%, $P = 0.014$), median overall survival (median survival of 9.5 months versus 5 months, $P = 0.025$), and less central nervous system (CNS) related deaths than the afternoon group ($P = 0.026$) [43]. Therefore, the role of circadian genes in cancers should be further investigated to provide new insight for the design of future treatment.

In this study, the prognostic efficacy of DEMIs were also analyzed. As for downstream miRNAs of hsa_circ_0072309, this study's results revealed that hsa-miR-34a, which was identified to bind to hsa_circ_0072309 using AGO2-RIP and dual-luciferase reporter assays, was up-regulated in GC. Moreover, the effects of different gene expression levels on the survival and prognosis of patients with GC were statistically different. To the best of this research group's knowledge, this is the first study reporting on the role of hsa-miR-34a in cancer. Interestingly, this study's findings showed that its overexpression in GC was related to a better prognosis, suggesting that hsa-miR-34a might be a novel prognostic biomarker.

As for the downstream mRNAs of hsa_circ_0072309, C7 was down-regulated in GC, and its expression level was significantly related to prognosis and immune infiltration. The mRNA C7 is a terminal ingredient of the complement cascade, and its insertion into the lipid bilayer is a crucial limiting step for the formation of the membrane attack complex (MAC) [44], which can be triggered by the complement system; it also exerts the effect of cytolysis, playing an essential role in immune surveillance and homeostasis [45,46]. Some studies have suggested that C7 may be a potential tumor suppressor. Oka et al. [47] found that C7 was prominently low-expressed in esophageal cancer tissues. Ying et al. [48] found that the expression of C7 decreased gradually in normal, benign, borderline, and malignant ovarian tissue; the down-regulation of C7 was associated with a low degree of differentiation in ovarian cancer tissue. A similar expression pattern was observed in normal tissues, paracancerous tissues, and malignant tissues of patients with NSCLC, and the low expression of C7 was related to an advanced clinical stage and a worse grade, indicating a poor outcome. Additionally, a multivariate Cox regression analysis showed that C7 was an independent predictor of prognosis in patients with NSCLC, and in vitro experiments indicated that a high expression of C7 inhibited the growth of NSCLC cells. The results of these studies were

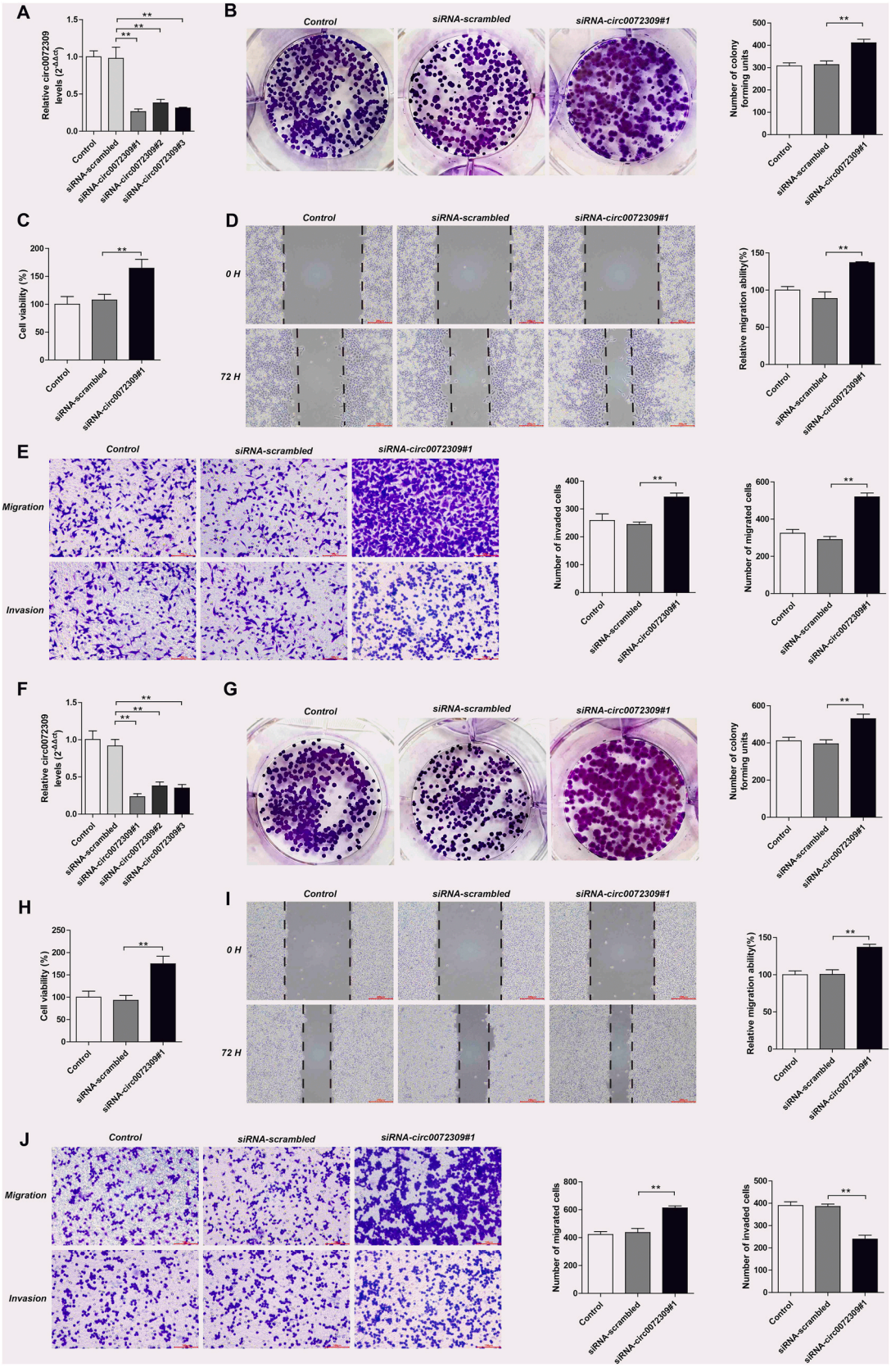

(caption on next page)

Fig. 8. Hsa_circ_0072309 knockdown promoted the malignant phenotype of the AGS (A–E) and MKN-45 (F–J) cell lines. Both cell lines were transfected with siRNA-scrambled, siRNA-circ0072309#1, siRNA-circ0072309#2, or siRNA-circ0072309#3. Polymerase chain reaction showed the knockdown efficiency in the AGS cells (A) and the MKN-45 cells (F), and siRNA-circ0072309#1 showed the best knockdown efficiency. (B) The colony formation assay of hsa_circ_0072309 knockdown in the AGS cells. (C) The cell viability of the hsa_circ_0072309 knockdown in the AGS cells was detected by a Cell Counting Kit-8 (CCK-8). (D) The lateral migration ability of the hsa_circ_0072309 knockdown in the AGS cells was measured by wound healing assays. (E) The migration and invasion abilities of the hsa_circ_0072309 knockdown in the AGS cells were analyzed by transwell assays. (G) The colony formation assay of the hsa_circ_0072309 knockdown in the MKN-45 cells. (H) The cell viability of the hsa_circ_0072309 knockdown in the MKN-45 cells was detected by a CCK-8. (I) The lateral migration ability of the hsa_circ_0072309 knockdown in the MKN-45 cells was measured by wound healing assays. (J) The migration and invasion abilities of the hsa_circ_0072309 knockdown in the MKN-45 cells were analyzed by transwell assays. All results are presented as the mean ± standard deviation for three individual experiments. $^{*}P < 0.05$, $^{**}P < 0.01$.

consistent with the conclusions of this study's analysis. As the complement system is an integral part of the inflammatory response, carcinogenic inflammation plays an essential role in tumor occurrence and development [49]. As was mentioned above, C7 is vital in cytolysis as an essential ingredient in the formation of MAC. It has been reported that sublytic MAC may impact tumor cell (colon carcinoma cell CT26 and melanoma cell B16) survival and proliferation and reshape the surrounding extracellular matrix [50]. In addition, the complement cascade can directly lyse malignant cells and enhance the killing effect of antibody-dependent cell-mediated cytotoxicity on tumor cells [46]. Complement activation, which simultaneously regulates an adaptive immune response, may regulate the T cell response to tumors [51]. This finding was also validated in our study by assessing the correlation between C7 and immune cell infiltration. This study's findings indicated a significant positive correlation between C7 expression and $CD8^+$ T cells, $CD4^+$ T cells, B cells, macrophages, neutrophils, and dendritic cells. In conclusion, C7 may act as a cancer suppressor in the process of tumorigenesis and progression, and it has the potential to predict the prognosis for tumor patients, making it a new therapeutic target.

5. Conclusion

Several limitations in this study should be noted. First, although the bioinformatics analyses and functional experiments were performed to identify the potential role of hsa_circ_0072309 in GC, additional in vivo experiments are required to validate the interaction of DEGs and explain their functions, including expression verification of the target miRNAs of hsa_circ_0072309 and molecules related to GO and KEGG functional analysis. Second, it is necessary to expand the sample size to further evaluate the effect of hsa_circ_0072309 expression on the development of the preoperative strategy and postoperative LNM monitoring in GC. Third, hsa_circ_0072309 expression was validated in GC tissues and cell lines; however, as an evaluation method, the implementation is limited by complex sampling. Additional studies on the differences of hsa_circ_0072309 expression in the serum between patients with GC and healthy subjects should be completed to determine whether the sensitivity is high enough in the serum to develop a non-invasive detection method. CIBERSOFT and Timer are online tools that use public databases to deconvolve transcriptomic data, thus, the correlation between immune infiltrates and gene expressions did not prove convincing since immune infiltrates might be originally correlated with gene expressions. Because there is no corresponding prognosis data for circRNA sequencing samples, and the follow-up period we collect patient information is relatively long, we cannot analyze the relationship between hsa_circ_0072309 and disease prognosis in this study, which is also a shortage of this study and our regret.

In conclusion, DECs were screened using online databases and this group's previous sequencing data, and the expression and survival prognosis of the intersected target genes were analyzed. The function of these DEGs were analyzed, and their correlation with immune infiltration was assessed. Concurrently, this study validated the expression of hsa_circ_0072309 both in vivo and in vitro and investigated the correlation between the expression level and the clinical characteristics of patients. In addition, this study evaluated the function of hsa_circ_0072309 and identified the binding sites between hsa_circ_0072309 and its downstream miRNAs. The results of this study indicated that hsa_circ_0072309 may be a promising biomarker for diagnosing and predicting LNM in GC, and its downstream gene C7 may be a tumor suppressor, which can help predict the prognosis of diagnosed patients. To the knowledge of this research group, this is the first study to make a detailed analysis of hsa_circ_0072309 to date, and its results will provide valuable insights into the diagnosis and treatment of GC by circRNA. However, more in vitro studies and animal experiments are needed to validate these conclusions.

Author contribution statement

Bei-Bei Xu: Conceived and designed the experiments; Contributed reagents, materials, analysis tools or data; Wrote the paper.
Yi Huang: Contributed reagents, materials, analysis tools or data; Wrote the paper.
En-Dian Zheng; Wen-Sheng Pan: Conceived and designed the experiments.
Jing-Ya Wang; Ya-Nan Wang: Performed the experiments.
Chen-Jing Zhang; Xiao-Ge Geng: Analyzed and interpreted the data.

Funding statement

Dr. Wen-Sheng Pan was supported by Zhejiang medicine key scientific and technology project [2018258924].
Chen-Jing Zhang was supported by Medical Science and Technology Project of Zhejiang Province [2019RC094].
Dr. Bei-Bei Xu was supported by Science and Technology Bureau of Wenzhou city [Y20220875].

Data availability statement

Data included in article/supp. material/referenced in article.

Declaration of interest's statement

The authors declare no competing interests.

Appendix A. Supplementary data

Supplementary data related to this article can be found at https://doi.org/10.1016/j.heliyon.2023.e13191.

References

[1] G. Luo, Y. Zhang, P. Guo, L. Wang, Y. Huang, K. Li, Global patterns and trends in stomach cancer incidence: age, period and birth cohort analysis, Int. J. Cancer 141 (7) (2017 Oct 1) 1333–1344, https://doi.org/10.1002/ijc.30835.

[2] F. Bray, J. Ferlay, I. Soerjomataram, R.L. Siegel, L.A. Torre, A. Jemal, Global cancer statistics 2018: GLOBOCAN estimates of incidence and mortality worldwide for 36 cancers in 185 countries, CA Cancer J Clin 68 (6) (2018 Nov) 394–424, https://doi.org/10.3322/caac.21492. PMID: 30207593].

[3] A. Veitch, N. Uedo, K. Yao, J. East, Veitch AM, Uedo N, Yao K, East JE. Optimizing early upper gastrointestinal cancer detection at endoscopy, Nat. Rev. Gastroenterol. Hepatol. 12 (11) (2015) 660–667, https://doi.org/10.1038/nrgastro.2015.128.

[4] Y.C. Lee, T.H. Chiang, C.K. Chou, Y.K. Tu, W.C. Liao, M.S. Wu, D.Y. Graham, Association between Helicobacter pylori eradication and gastric cancer incidence: a systematic review and meta-analysis, Gastroenterology 150 (5) (2016 May) 1113–1124, https://doi.org/10.1053/j.gastro.2016.01.028, e5 [doi:.

[5] J. Liu, T. Liu, X. Wang, A. He, Circles reshaping the RNA world: from waste to treasure, Mol. Cancer 16 (1) (2017 Mar 9) 58, https://doi.org/10.1186/s12943-017-0630-y.

[6] Y. Ruan, Z. Li, Y. Shen, T. Li, H. Zhang, J. Guo, Functions of circular RNAs and their potential applications in gastric cancer, Expet Rev. Gastroenterol. Hepatol. 14 (2) (2020 Feb) 85–92, https://doi.org/10.1080/17474124.2020.1715211.

[7] L. Peng, H. Sang, S. Wei, Y. Li, D. Jin, X. Zhu, X. Li, Y. Dang, G. Zhang, circCUL2 regulates gastric cancer malignant transformation and cisplatin resistance by modulating autophagy activation via miR-142-3p/ROCK2, Mol. Cancer 19 (1) (2020 Nov 5) 156, https://doi.org/10.1186/s12943-020-01270-x.

[8] D. Rong, C. Lu, B. Zhang, K. Fu, S. Zhao, W. Tang, H. Cao, Correction to: CircPSMC3 suppresses the proliferation and metastasis of gastric cancer by acting as a competitive endogenous RNA through sponging miR-296-5p, Mol. Cancer 19 (1) (2020 Sep 9) 140, https://doi.org/10.1186/s12943-020-01252-z.

[9] D. Rong, C. Dong, K. Fu, H. Wang, W. Tang, H. Cao, Upregulation of circ_0066444 promotes the proliferation, invasion, and migration of gastric cancer cells, OncoTargets Ther. 11 (2018 May 11) 2753–2761, https://doi.org/10.2147/OTT.S156516.

[10] C. Zhang, J. Wang, X. Geng, J. Tu, H. Gao, L. Li, X. Zhou, H. Wu, J. Jing, W. Pan, Y. Mou, Circular RNA expression profile and m6A modification analysis in poorly differentiated adenocarcinoma of the stomach, Epigenomics 12 (12) (2020 Jun) 1027–1040, https://doi.org/10.2217/epi-2019-0153.

[11] X. Guo, M. Qin, H. Hong, X. Xue, J. Fang, L. Jiang, Y. Kuang, L. Gao, Circular RNA hsa_circ_0072309 inhibits the proliferation, invasion and migration of gastric cancer cells via inhibition of PI3K/AKT signaling by activating PPARγ/PTEN signaling, Mol. Med. Rep. 23 (5) (2021 May) 349, https://doi.org/10.3892/mmr.2021.11988.

[12] M.J. Goldman, B. Craft, M. Hastie, K. Repečka, F. McDade, A. Kamath, A. Banerjee, Y. Luo, D. Rogers, A.N. Brooks, J. Zhu, D. Haussler, Visualizing and interpreting cancer genomics data via the Xena platform, Nat. Biotechnol. 38 (6) (2020 Jun) 675–678, https://doi.org/10.1038/s41587-020-0546-8.

[13] M.E. Ritchie, B. Phipson, D. Wu, Y. Hu, C.W. Law, W. Shi, G.K. Smyth, Limma powers differential expression analyses for RNA-sequencing and microarray studies, Nucleic Acids Res 43 (7) (2015 Apr 20) e47, https://doi.org/10.1093/nar/gkv007.

[14] S. Xia, J. Feng, K. Chen, Y. Ma, J. Gong, F. Cai, Y. Jin, Y. Gao, L. Xia, H. Chang, L. Wei, L. Han, C. He, CSCD: a database for cancer-specific circular RNAs, Nucleic Acids Res 46 (D1) (2018 Jan 4) D925–D929, https://doi.org/10.1093/nar/gkx863.

[15] M. Liu, Q. Wang, J. Shen, B.B. Yang, Ding X. Circbank, A comprehensive database for circRNA with standard nomenclature, RNA Biol. 16 (7) (2019 Jul) 899–905, https://doi.org/10.1080/15476286.2019.1600395.

[16] V. Agarwal, G.W. Bell, J.W. Nam, D.P. Bartel, Predicting effective microRNA target sites in mammalian mRNAs, Elife 4 (2015 Aug 12), e05005, https://doi.org/10.7554/eLife.05005. PMID: 26267216].

[17] X. Meng, D. Hu, P. Zhang, Q. Chen, M. Chen, CircFunBase: a database for functional circular RNAs, Database (2019) baz003, https://doi.org/10.1093/database/baz003.

[18] N.T. Doncheva, J.H. Morris, J. Gorodkin, L.J. Jensen, Cytoscape StringApp: network analysis and visualization of proteomics data, J. Proteome Res. 18 (2) (2019 Feb 1) 623–632, https://doi.org/10.1021/acs.jproteome.8b00702.

[19] H.Y. Huang, Y.C. Lin, J. Li, K.Y. Huang, S. Shrestha, H.C. Hong, Y. Tang, Y.G. Chen, C.N. Jin, Y. Yu, J.T. Xu, Y.M. Li, X.X. Cai, Z.Y. Zhou, X.H. Chen, Y.Y. Pei, L. Hu, J.J. Su, S.D. Cui, F. Wang, Y.Y. Xie, S.Y. Ding, M.F. Luo, C.H. Chou, N.W. Chang, K.W. Chen, Y.H. Cheng, X.H. Wan, W.L. Hsu, T.Y. Lee, F.X. Wei, H. D. Huang, miRTarBase 2020: updates to the experimentally validated microRNA-target interaction database, Nucleic Acids Res 48 (D1) (2020 Jan 8) D148–D154, https://doi.org/10.1093/nar/gkz896.

[20] S. Griffiths-Jones, R.J. Grocock, S. van Dongen, A. Bateman, A.J. Enright, miRBase: microRNA sequences, targets and gene nomenclature, Nucleic Acids Res 34 (2006 Jan 1) D140–D144, https://doi.org/10.1093/nar/gkj112 (Database issue).

[21] A.J. Enright, B. John, U. Gaul, T. Tuschl, C. Sander, D.S. Marks, MicroRNA targets in Drosophila, Genome Biol 5 (1) (2003) R1, https://doi.org/10.1186/gb-2003-5-1-r1.

[22] G. Dennis Jr., B.T. Sherman, D.A. Hosack, J. Yang, W. Gao, H.C. Lane, R.A. Lempicki, DAVID: database for annotation, visualization, and integrated discovery, Genome Biol 4 (5) (2003). P3 [PMID: 12734009].

[23] G. Bindea, B. Mlecnik, H. Hackl, P. Charoentong, M. Tosolini, A. Kirilovsky, W.H. Fridman, F. Pagès, Z. Trajanoski, J. Galon, ClueGO: a Cytoscape plug-in to decipher functionally grouped gene ontology and pathway annotation networks, Bioinformatics 25 (8) (2009 Apr 15) 1091–1093, https://doi.org/10.1093/bioinformatics/btp101.

[24] A.M. Newman, C.L. Liu, M.R. Green, A.J. Gentles, W. Feng, Y. Xu, C.D. Hoang, M. Diehn, A.A. Alizadeh, Robust enumeration of cell subsets from tissue expression profiles, Nat. Methods 12 (5) (2015 May) 453–457, https://doi.org/10.1038/nmeth.3337.

[25] T. Li, J. Fan, B. Wang, N. Traugh, Q. Chen, J.S. Liu, B. Li, X.S. Liu, TIMER: a web server for comprehensive analysis of tumor-infiltrating immune cells, Cancer Res. 77 (21) (2017 Nov 1) e108–e110, https://doi.org/10.1158/0008-5472.CAN-17-0307. PMID: 29092952].

[26] K.J. Livak, T.D. Schmittgen, Analysis of relative gene expression data using real-time quantitative PCR and the 2(-Delta Delta C(T)) Method, Methods 25 (4) (2001 Dec) 402–408, https://doi.org/10.1006/meth.2001.1262.

[27] H. Katai, T. Ishikawa, K. Akazawa, Y. Isobe, I. Miyashiro, I. Oda, S. Tsujitani, H. Ono, S. Tanabe, T. Fukagawa, S. Nunobe, Y. Kakeji, A. Nashimoto, Registration Committee of the Japanese Gastric Cancer Association. Five-year survival analysis of surgically resected gastric cancer cases in Japan: a retrospective analysis of

more than 100,000 patients from the nationwide registry of the Japanese Gastric Cancer Association (2001-2007), Gastric Cancer 21 (1) (2018 Jan) 144–154, https://doi.org/10.1007/s10120-017-0716-7.
[28] L. Yan, M. Zheng, H. Wang, Circular RNA hsa_circ_0072309 inhibits proliferation and invasion of breast cancer cells via targeting miR-492, Cancer Manag. Res. 11 (2019 Jan 22) 1033–1041, https://doi.org/10.2147/CMAR.S186857. PMID: 30774431].
[29] L. Yang, W. Tan, Y. Wei, Z. Xie, W. Li, X. Ma, Q. Wang, H. Li, Z. Zhang, C. Shang, Y. Chen, CircLIFR suppresses hepatocellular carcinoma progression by sponging miR-624-5p and inactivating the GSK-3β/β-catenin signaling pathway, Cell Death Dis. 13 (5) (2022 May 17) 464, https://doi.org/10.1038/s41419-022-04887-6.
[30] Y. Zhou, Z. Tong, X. Zhu, S. Huang, Z. Dong, Z. Ye, hsa_circ_0072309 expression profiling in non-small-cell lung carcinoma and its implications for diagnosis and prognosis, Front Surg 9 (2022 Feb 25), 842292, https://doi.org/10.3389/fsurg.2022.842292.
[31] C.L. Chaffer, R.A. Weinberg, A perspective on cancer cell metastasis, Science 331 (6024) (2011 Mar 25) 1559–1564, https://doi.org/10.1126/science.1203543.
[32] C.L. Dai, Z.G. Yang, L.P. Xue, Y.M. Li, Application value of multi-slice spiral computed tomography for imaging determination of metastatic lymph nodes of gastric cancer, World J. Gastroenterol. 19 (34) (2013 Sep 14) 5732–5737, https://doi.org/10.3748/wjg.v19.i34.5732.
[33] H. Deng, R.L. Wu, H.Y. Zhou, X. Huang, Y. Chen, L.J. Liu, Significance of Survivin and PTEN expression in full lymph node-examined gastric cancer, World J. Gastroenterol. 12 (7) (2006 Feb 21) 1013–1017, https://doi.org/10.3748/wjg.v12.i7.1013.
[34] X. Wei, Y.B. Li, Y. Li, B.C. Lin, X.M. Shen, R.L. Cui, Y.J. Gu, M. Gao, Y.G. Li, S. Zhang, Prediction of lymph node metastases in gastric cancer by serum APE1 expression, J. Cancer 8 (8) (2017 Jun 1) 1492–1497, https://doi.org/10.7150/jca.18615.
[35] D. Hanahan, R.A. Weinberg, The hallmarks of cancer, Cell 100 (1) (2000 Jan 7) 57–70, https://doi.org/10.1016/s0092-8674(00)81683-9.
[36] B. Srour, S. Plancoulaine, V.A. Andreeva, P. Fassier, C. Julia, P. Galan, S. Hercberg, M. Deschasaux, P. Latino-Martel, M. Touvier, Circadian nutritional behaviours and cancer risk: new insights from the NutriNet-santé prospective cohort study: disclaimers, Int. J. Cancer 143 (10) (2018 Nov 15) 2369–2379, https://doi.org/10.1002/ijc.31584.
[37] M.G. Wendeu-Foyet, F. Menegaux, Circadian disruption and prostate cancer risk: an updated review of epidemiological evidences, Cancer Epidemiol. Biomarkers Prev. 26 (7) (2017 Jul) 985–991, https://doi.org/10.1158/1055-9965.
[38] S.C. Markt, E.E. Flynn-Evans, U.A. Valdimarsdottir, L.G. Sigurdardottir, R.M. Tamimi, J.L. Batista, S. Haneuse, S.W. Lockley, M. Stampfer, K.M. Wilson, C. A. Czeisler, J.R. Rider, L.A. Mucci, Sleep duration and disruption and prostate cancer risk: a 23-year prospective study, Cancer Epidemiol. Biomarkers Prev. 25 (2) (2016 Feb) 302–308, https://doi.org/10.1158/1055-9965.EPI-14-1274. PMID: 26677208].
[39] A.A. Shafi, K.E. Knudsen, Cancer and the circadian clock, Cancer Res. 79 (15) (2019 Aug 1) 3806–3814, https://doi.org/10.1158/0008-5472.CAN-19-0566.
[40] C.H. Jung, E.M. Kim, J.K. Park, S.G. Hwang, S.K. Moon, W.J. Kim, H.D. Um, Bmal1 suppresses cancer cell invasion by blocking the phosphoinositide 3-kinase-Akt-MMP-2 signaling pathway, Oncol. Rep. 29 (6) (2013 Jun) 2109–2113, https://doi.org/10.3892/or.2013.2381.
[41] M. Kobayashi, P.A. Wood, W.J. Hrushesky, Circadian chemotherapy for gynecological and genitourinary cancers, Chronobiol. Int. 19 (1) (2002 Jan) 237–251, https://doi.org/10.1081/cbi-120002600.
[42] F. Lévi, R. Zidani, J.L. Misset, Randomised multicentre trial of chronotherapy with oxaliplatin, fluorouracil, and folinic acid in metastatic colorectal cancer. International Organization for Cancer Chronotherapy, Lancet 350 (9079) (1997 Sep 6) 681–686, https://doi.org/10.1016/s0140-6736(97)03358-8.
[43] D.A. Rahn 3rd, D.K. Ray, D.J. Schlesinger, L. Steiner, J.P. Sheehan, J.M. O'Quigley, T. Rich, Gamma knife radiosurgery for brain metastasis of nonsmall cell lung cancer: is there a difference in outcome between morning and afternoon treatment? Cancer 117 (2) (2011 Jan 15) 414–420, https://doi.org/10.1002/cncr.25423.
[44] R. Würzner, Modulation of complement membrane attack by local C7 synthesis, Clin. Exp. Immunol. 121 (1) (2000 Jul) 8–10, https://doi.org/10.1046/j.1365-2249.2000.01263.x.
[45] D. Ricklin, G. Hajishengallis, K. Yang, J.D. Lambris, Complement: a key system for immune surveillance and homeostasis, Nat. Immunol. 11 (9) (2010 Sep) 785–797, https://doi.org/10.1038/ni.1923.
[46] M. Serna, J.L. Giles, B.P. Morgan, D. Bubeck, Structural basis of complement membrane attack complex formation, Nat. Commun. 7 (2016 Feb 4), 10587, https://doi.org/10.1038/ncomms10587.
[47] R. Oka, T. Sasagawa, I. Ninomiya, K. Miwa, H. Tanii, K. Saijoh, Reduction in the local expression of complement component 6 (C6) and 7 (C7) mRNAs in oesophageal carcinoma, Eur. J. Cancer 37 (9) (2001 Jun) 1158–1165, https://doi.org/10.1016/s0959-8049(01)00089-2.
[48] L. Ying, F. Zhang, X. Pan, K. Chen, N. Zhang, J. Jin, J. Wu, J. Feng, H. Yu, H. Jin, D. Su, Complement component 7 (C7), a potential tumor suppressor, is correlated with tumor progression and prognosis, Oncotarget 7 (52) (2016 Dec 27) 86536–86546, https://doi.org/10.18632/oncotarget.13294.
[49] L.M. Coussens, L. Zitvogel, A.K. Palucka, Neutralizing tumor-promoting chronic inflammation: a magic bullet? Science 339 (6117) (2013 Jan 18) 286–291, https://doi.org/10.1126/science.1232227.
[50] L.D. Towner, R.A. Wheat, T.R. Hughes, B.P. Morgan, Complement membrane attack and tumorigenesis: a systems biology approach, J. Biol. Chem. 291 (29) (2016 Jul 15) 14927–14938, https://doi.org/10.1074/jbc.M115.708446.
[51] V. Afshar-Kharghan, The role of the complement system in cancer, J. Clin. Invest. 127 (3) (2017 Mar 1) 780–789, https://doi.org/10.1172/JCI90962.